Purdue University
Purdue e-Pubs

International Refrigeration and Air Conditioning Conference

School of Mechanical Engineering

2012

Dynamic Model for Small-Scale Ammonia-Water Absorption Chiller

Vinodh K. Viswanathan
sgarimella@gatech.edu

Alexander S. Rattner

Matthew D. Determan

Srinivas Garimella

Follow this and additional works at: http://docs.lib.purdue.edu/iracc

Dynamic Model for Small-Capacity Ammonia-Water Absorption Chiller

Vinodh K. Viswanathan, Alexander S. Rattner, Matthew D. Determan, and Srinivas Garimella*****

Sustainable Thermal Systems Laboratory
George W. Woodruff School of Mechanical Engineering
Georgia Institute of Technology
Atlanta, GA 30032
(404) 894-7479; sgarimella@gatech.edu

*Corresponding Author

ABSTRACT

Optimization of the performance of absorption systems during transient operations such as start-up and shut-down to minimize lifetime costs is particularly important for small-capacity chillers and heat pumps. Most dynamic models in the literature have analyzed the transient response for a step change in a single parameter, but few have explored entire start-up and shut-down processes and control strategies. An accurate and robust model for simulating the transient behavior of an absorption chiller was developed here. The individual heat exchangers in the absorption system were analyzed using detailed segmental models. In components with significant mass transfer effects, reduced-order models are employed to decrease computational costs while also maintaining accurate system responses. System parameters such as heat exchanger size, solution flow rates, coupling fluid temperatures and flow rates used in the model are representative of a practical absorption chiller under development by the authors. This analysis can be used to minimize start-up times and also enhance steady state performance. The model can also be used for devising and testing control strategies in commercial applications.

1. INTRODUCTION

Absorption cycles have been employed in refrigeration and air-conditioning for many years, but have attracted renewed interest in recent years due to environmental concerns such as global climate change and ozone depletion. The ammonia-water fluid pair has extremely low ODP and GWP values compared to conventional refrigerants such as HCFCs and CFCs, which are typically used in vapor-compression systems. Also, vapor-compression systems require high-grade electricity to power a compressor and produce cooling or heating. In contrast, absorption systems are primarily thermally activated, and can use abundant low-grade waste-heat, such as engine exhaust, to deliver cooling or heating. However, absorption systems require additional components compared to vapor-compression systems and therefore could have larger capital costs. When installed in a typical application, a small capacity absorption chiller may experience multiple start-up and shut-down events daily, and must respond to continuously varying ambient conditions and cooling loads. Without active system management, such transient operating conditions can lead to a significant loss of performance. Robust control strategies must be developed to minimize these losses and improve overall chiller performance. The control system should constantly interact with various components of the chiller, monitor temperatures, pressures, and other key properties, and select an appropriate set of control parameters such as valve positions and fan and pump speeds. A study of system behavior during start-up, shut-down, and changes in environmental conditions can assist in the development of control algorithms. Start-up behavior of a 3.5 kW cooling capacity absorption chiller is presented here.

Several studies have investigated the dynamic behavior of absorption chillers and heat pumps. Kaushik *et al.* (1985) simulated the dynamic performance of a solar driven heat pump accounting for ammonia-water storage using two different storage tanks. Mass and species storage were modeled primarily through the storage tanks, and lumped-capacity models were used to model heat transfer in other components. Lumped capacity component models for the overall heat transfer are not sufficient for capturing the transient heat transfer processes envisioned in this miniaturized absorption system (Determan and Garimella, 2012). Jeong *et al.* (1998) conducted a numerical study of the dynamic performance of a single-effect LiBr-H_2O absorption heat pump. The effects of different parameters including flow rates, temperatures of coupling fluids, and heat exchanger areas were analyzed in detail. Fu *et al.* (2006) developed an object-oriented simulation tool, ABSML (Absorption System Modeling Library) for dynamic

absorption systems. Using this tool, heat and mass transfer components were simulated using lumped capacity models, and a perturbation analysis was performed around steady state to study transient behavior. However, refrigerant and solution storage in the cycle was modeled primarily in the heat transfer components, and no specific device was incorporated to store any excess solution or refrigerant. Kim and Park (2007) performed a numerical study on the dynamic response of single-effect ammonia-water systems. The study focused on absorption system start-up as well as device response to step changes in flue-gas flow rate. However, their model included thermal energy storage only for the desorber, and neglected the thermal masses of other components in the cycle. Also, their model used a lumped-capacity approach, and each component was characterized by a single temperature value. Kohlenbach and Ziegler (2008) performed a dynamic simulation of a single-effect LiBr-H$_2$O system. Their model accounted for the effects of transient behavior from factors such as transient mass storage in the absorber and desorber, thermal energy storage in all components, and a solution transport delay. Their dynamic simulations were shown to match closely with experiments. Cai *et al.* (2011) simulated the dynamic response of a single-effect ammonia-water absorption cycle to a step change in the solution pump pressure rise. However, their simplified model assumed pure ammonia flow in the refrigerant loop, and employed a quadratic curve fit to correlate the low-to-high side pressure differential and solution flow rate.

To date, most studies have relied on lumped-capacity assumptions for the components. However, temperature variation inside components may be significant, especially during transient operation due to thermal transport delays. To capture such transient behavior accurately, segmented modeling of the heat and mass exchanging components is employed here. The thermal storage capacity of individual components significantly affects the transient behavior of the system and is also accounted for in the present model. Also, while many studies have modeled the pressure difference across system components using momentum balances, few have accounted for the transient pressure variations driven by mass accumulation in the system storage devices that have a much larger influence on system behavior. In a system with miniaturized heat and mass exchangers, the solution and refrigerant storage tanks account for the major portion of the fluid inventory. Thus, vapor-liquid equilibrium conditions in these components control the system pressures. Accurate models for high- and low-side pressure variations are required for predicting flow rates and overall system behavior. The robust and detailed model developed here will enable simulation of the entire start-up and shut-down processes, not only responses to step changes in a single parameter.

2. SYSTEM ARCHITECTURE AND SPECIFICATIONS

A dynamic model for a single-effect ammonia-water absorption cycle is developed in this study to address some of the limitations of other similar efforts discussed above. Key system parameters such as heat exchanger sizes, valve restrictions, solution flow rates, pumping rate, volume of solution and refrigerant stored in the cycle, are representative of a miniaturized absorption chiller being developed by the authors. Transient behavior during start-up is modeled accounting for thermal mass of the heat and mass exchanging components, gradual pressure evolution in the system, and flow rates driven by pressure differentials across system expansion valves. Heat and mass exchanger walls are assigned appropriate thermal capacities, and adjacent fluid volumes are also capable of energy storage. The heat exchangers are divided into segments to enable accurate prediction of heat transfer and thermal energy storage. Flow rates and species concentrations are assumed to be uniform in individual segments. By using smaller segments for components, model precision can be increased if necessary. System pressures are determined from vapor-liquid equilibrium conditions in the storage tanks. The high-pressure components (desorber, rectifier, condenser and SHX) are assumed to be at the pressure set by the refrigerant tank fed from the condenser outlet. Frictional
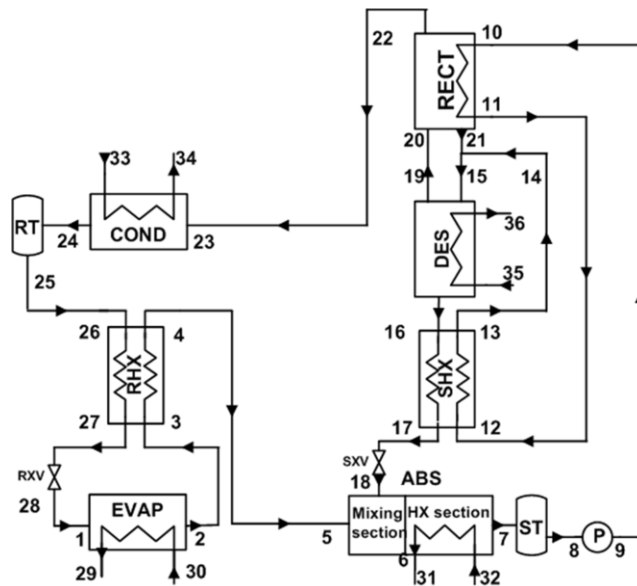

Figure 1: Absorption cycle - schematic

pressure drops in the components are assumed to be negligible compared to an approximately 1.5 MPa difference between high- and low-side system pressures. The low-pressure components (evaporator and absorber) are assumed to be at the pressure set by the solution tank fed from the absorber outlet. Storage of refrigerant and solution is assumed to occur solely in the refrigerant and solution tanks, respectively, because the microchannel heat and mass exchangers employed in the miniaturized heat pump have minimal fluid inventories. The model is developed in the Simulink® environment and components are modeled as individual blocks and integrated to form a closed cycle. Figure 1 presents a schematic of the single-effect ammonia-water absorption cycle considered in this study. The basic components of the cycle are the evaporator (EVAP), condenser (COND), desorber (DES), absorber (ABS), solution tank (ST) and refrigerant tank (RT). The recuperative heat exchangers include the solution heat exchanger (SHX), refrigerant heat exchanger (RHX), and rectifier (RECT). Other components, such as the solution pump (P) and expansion valve (EV) are also included.

3. DYNAMIC MODEL FORMULATION

3.1 Heat Exchanger Model

To estimate heat transfer in the heat exchanging components, such as the evaporator, condenser and absorber, a segmented counterflow model is developed. Each such component is divided into N equal segments. A single segment comprises an internal dividing wall and two adjacent fluid volumes. Each wall segment is assigned a thermal capacity ($m \cdot c_p$) and thermal energy storage is tracked in each fluid segment.

Figure **2** shows a schematic of a heat exchanger where fluids 1 and 2 are in a counterflow arrangement. The discretization is shown for a heat exchanger with *N* segmental control volumes.

Figure **3** shows the control volumes for the wall and fluids, corresponding to the ith segment of the heat-exchanger component. The heat transfer is modeled as shown in Equations ((1)-(4)).

$$. \frac{dU_{1f,i}}{dt} = \dot{m}_{1f} \cdot (h_{1f,in} - h_{1f,out}) - \dot{Q}_{1f,i} . \tag{1}$$

$$\frac{dU_{2f,i}}{dt} = \dot{Q}_{2f,i} - \dot{m}_{2f,i} \cdot (h_{2f,out} - h_{2f,in}) \tag{2}$$

$$(M.c_p)_{w,i} \cdot \frac{dT_{w,i}}{dt} = \dot{Q}_{1f,i} - \dot{Q}_{2f,i} \tag{3}$$

Here the enthalpies at the inlet and outlet are evaluated using a first-order upwind scheme (Patankar, 1980).

$$h_{1f,in} = h_{1f,i-1}, \quad h_{1f,out} = h_{1f,i}$$
$$h_{2f,in} = h_{2f,i+1}, \quad h_{2f,out} = h_{2f,i} \tag{4}$$

The internal heat transfer rates $\dot{Q}_{1f,i}$ and $\dot{Q}_{2f,i}$ in the ith segment are expressed in terms of the fluid temperatures ($T_{1f,i}$, $T_{2f,i}$), wall temperature $T_{w,i}$, and their respective heat transfer coefficients and transfer areas ($\alpha A_{1f,i}$), ($\alpha A_{2f,i}$) as shown in Equation (5).

$$\dot{Q}_{1f,i} = (\alpha A)_{1f,i} \cdot (T_{1f,i} - T_{w,i}), \quad \dot{Q}_{2f,i} = (\alpha A)_{2f,i} \cdot (T_{w,i} - T_{2f,i}) \tag{5}$$

For components such as the evaporator, condenser and absorber, 1f represents the ammonia-water mixture and 2f represents the coupling fluid whereas for SHX and RHX, both 1f and 2f represent the ammonia-water mixture. For the ammonia-water mixture, internal energy and specific enthalpy are evaluated using: $U_{1f,i} = M_{1f,i}(h_{1f,i} - P_i v_{1f,i})$, while for the coupling fluids (single-phase liquids), they are evaluated as $U_{2f,i} = M_{2f,i} h_{2f,i}$. An initial mass of ammonia-water mixture M_{1f} is assumed to be present inside the component, based on the component fluid volume and an assumed initial density. The mass is equally divided in each of the *N* segments of the heat exchanger. Therefore the segmental mass $M_{1f,i}$ depends on the density of the fluid and volume of the segment ($M_{1f,i} = \rho_{1f} V_{HX,i}$).

Flow rates, thermal capacities, heat transfer resistances, and material properties are adopted from a previously developed steady-state system model. Specifications for the heat exchangers are summarized in Table 1.

Frictional pressure drops across components are assumed negligible compared to the low-to-high side pressure difference (~1.5 MPa in steady state). Thus, each segment pressure is set to the respective overall component pressure. Internal segmental mass and species storages are also neglected; therefore, the concentrations and flow
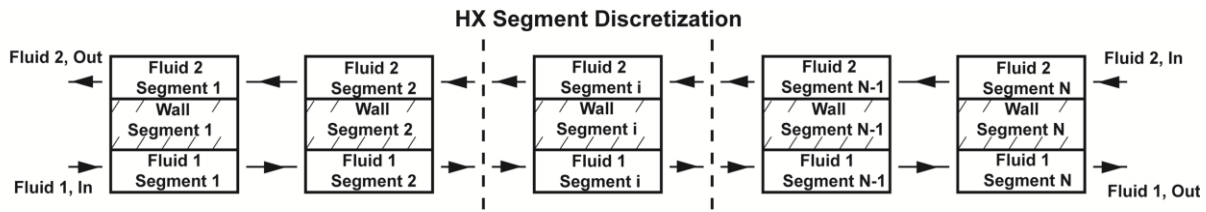
HX Segment Discretization

Figure 2: Discretized model of HX

rates of the ammonia-water mixture are assumed to be equal in all segments in each component. The microchannel heat and mass exchangers considered here are assumed to have negligible fluid inventories compared to the solution and refrigerant tanks. Once the inlet and outlet enthalpies are known, the component heat transfer rates are estimated between corresponding state points (Figure 1). During transient operation, the heat transfer rates for the two fluids in the SHX and RHX are different due to thermal storage in the HX wall.

$$\dot{Q}_{EVAP} = \dot{m}_1 \cdot (h_2 - h_1) \tag{6}$$

$$\dot{Q}_{COND} = \dot{m}_{23} \cdot (h_{24} - h_{23}) \tag{7}$$

$$\dot{Q}_{SHX,cool} = \dot{m}_{16} \cdot (h_{17} - h_{16}), \quad \dot{Q}_{SHX,heat} = \dot{m}_{12} \cdot (h_{13} - h_{12}) \tag{8}$$

$$\dot{Q}_{RHX,cool} = \dot{m}_{26} \cdot (h_{27} - h_{26}), \quad \dot{Q}_{RHX,heat} = \dot{m}_3 \cdot (h_4 - h_3) \tag{9}$$

$$\dot{Q}_{ABS} = \dot{m}_6 \cdot (h_7 - h_6) \tag{10}$$

The absorber is modeled as a combination of a pre-mixing section and a heat exchanger section. In the pre-mixing section, incoming ammonia vapor (5) and dilute ammonia-water solution (18) mix and reach thermal equilibrium (6) (Figure 1). The geometry of the absorber is assumed to thoroughly mix the liquid and vapor phases. The well-mixed fluid cools as it flows through the absorber heat exchanger section (Figure 1). The mass transfer resistance between the liquid and vapor in the absorber is neglected and heat transfer due to cooling and phase change of the liquid-vapor mixture is estimated as the heat load for the absorber.

The heat transfer process in the desorber involves a complex liquid-vapor interaction for the ammonia-water mixture (solution-side). In the counterflow desorber investigated here, liquid solution flows downward, countercurrent to rising refrigerant vapor. The liquid phase is heated by the hot desorber wall, generating vapor as it flows down. The desorber model is divided into three equal segments ($N = 3$). Figure 4(a) represents a counterflow desorber segment with downward flowing solution and rising ammonia-rich vapor. Figure 4(b) summarizes the heat transfer between the control volumes of ammonia-water (solution side), coupling fluid and the internal wall, for the ith segment. To reduce the complexity of the desorber model, the following assumptions are made:

- Thermal storage capacity in the ammonia-water mixture is negligible compared to that in the desorber wall and coupling fluid.
- The liquid and vapor phases are at saturated thermodynamic states throughout the desorber.

These assumptions simplify this system-level model, but future system models and more detailed component-level models may warrant more rigorous models that account for heat and mass transfer rates between the liquid and vapor phases. Properties (enthalpy, concentration, etc.) and flow rates at the segment boundaries are identical to the ones upstream of the
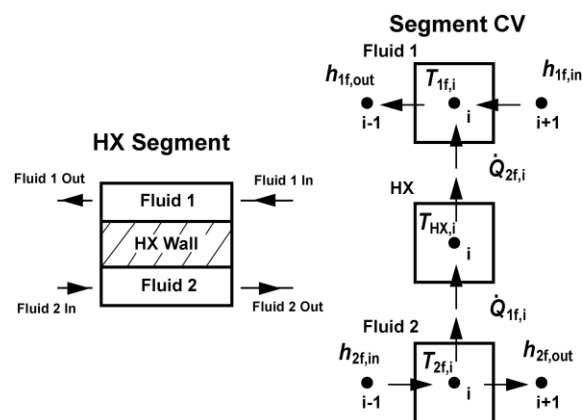

Figure 3: Segmental CV of HX

Table 1: Properties of EVAP, COND, ABS, DES, RHX and SHX

Description		Units	Parameter	Component					
				EVAP	COND	ABS	DES	SHX	RHX
Coupling fluid/fluid 2	Specific heat	kJ kg⁻¹ K⁻¹	$c_{p,cf}$	4.0	4.2	4.2	2.577	-	
	Density	kg m⁻³	ρ_{cf}	1000	1000	1000	890	800	
	Segmental volume	m³	$V_{cf,i}$	10^{-4}	10^{-4}	10^{-4}	10^{-4}	10^{-4}	
	Segmental mass	kg	$m_{cf,i}$	0.1	0.1	0.1	0.089	0.1	
	Flow rate	kg s⁻¹	$\dot{m}_{cf,i}$	0.16	0.112	0.112	0.084	-	
Wall	Specific heat	kJ kg⁻¹ K⁻¹	$c_{p,w}$	0.51				0.51	
	Segmental mass	kg	$m_{w,i}$	0.2				0.1	
Ammonia-water/fluid 1	Initial density	kg m⁻³	ρ_{sol}	800				800	
	Segmental volume	m³	$V_{sol,i}$	10^{-4}				10^{-4}	
	Segmental mass	kg	$m_{sol,i}$	0.08				0.1	
	No. of segments	-	N	5	5	5	3	3	3
	Heat transfer coefficient	W K⁻¹	$(\alpha A)_{f,i}$	450	170	320	600	360	525
	Heat transfer coefficient	W K⁻¹	$(\alpha A)_{cf,i}$	215	450	810	600	275	40

control volume, per the upwind scheme (Patankar, 1980). The governing mass, species and energy balance equations for the ammonia-water mixture (solution side CV) in each desorber segment are:

$$\dot{m}_{liq,i+1} + \dot{m}_{vap,i-1} = \dot{m}_{liq,i} + \dot{m}_{vap,i} \tag{11}$$

$$\dot{m}_{liq,i+1} \cdot X_{liq,i+1} + \dot{m}_{vap,i-1} \cdot X_{vap,i-1} = \dot{m}_{liq,i} \cdot X_{liq,i} + \dot{m}_{vap,i} \cdot X_{vap,i} \tag{12}$$

$$\dot{m}_{liq,i+1} \cdot h_{liq,i+1} + \dot{m}_{vap,i-1} \cdot h_{vap,i-1} + (\alpha A)_{liq,i} \cdot (T_{w,i} - T_{liq,i}) = \dot{m}_{liq,i} \cdot h_{liq,i} + \dot{m}_{vap,i} \cdot h_{vap,i} \tag{13}$$

The energy balance for the coupling fluid and internal dividing wall segments are:

$$(M \cdot c_p)_{cf} \cdot \frac{dT_{cf,i}}{dt} = \dot{m}_{cf} c_{p,cf} \cdot (T_{cf,i-1} - T_{cf,i}) - (\alpha A)_{cf,i} \cdot (T_{cf,i} - T_{w,i}) \tag{14}$$

$$(M \cdot c_p)_{w,i} \cdot \frac{dT_{w,i}}{dt} = (\alpha A)_{cf,i} \cdot (T_{cf,i} - T_{w,i}) - (\alpha A)_{liq,i} \cdot (T_{w,i} - T_{liq,i}) \tag{15}$$

The desorber segmental heat transfer coefficients and material properties are summarized in Table 1. Thus, there are eight unknowns for each solution-side segment in the desorber:
$(\dot{m}_{liq,i}, \dot{m}_{vap,i}, X_{liq,i}, X_{vap,i}, h_{liq,i}, h_{vap,i}, T_{liq,i}, T_{vap,i})$.

The liquid inlet conditions at the top of the desorber (concentrated solution inlet at 15 - Figure 1) are obtained from the SHX outlet, and because no vapor enters the desorber at the bottom, the bottom-most segment has a zero vapor inflow rate $(\dot{m}_{vap,0} = 0)$. The unknown desorber solution-side quantities are evaluated using the secant-method based solver described in the following section. This specialized solver was developed to reduce computation time compared to the Simulink® built-in solver. The guess values for the vapor and liquid outflow rates in a segment are set to the inflow values. The saturated vapor-phase concentration and enthalpy
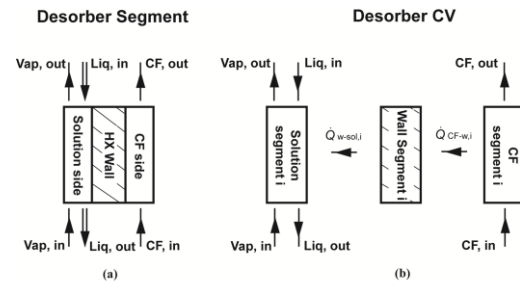
Figure 4(a): Segmented model of a desorber (b): CV of desorber

$(X_{\text{vap,i}}, h_{\text{vap,i}})$ are then evaluated using phase equilibrium relations at the vapor phase temperature $(T_{\text{vap,i}} = T_{\text{liq,i+1}})$ and inlet pressure specified at state point 15 (Figure 1). Mass and species balances (Equations (11) and (12)) are performed to determine the liquid-phase concentration $X_{\text{liq,i}}$. The saturated liquid-phase properties $(T_{\text{liq,i}}, h_{\text{liq,i}})$ are then evaluated using liquid-vapor equilibrium conditions at the liquid-phase concentration and pressure. Finally, the residual energy is evaluated from the energy balance on the solution side (Equation (17)) and is used to update the vapor flow rate.

$$\dot{m}_{\text{liq,i}} = \dot{m}_{\text{liq,i+1}} \, , \, \dot{m}_{\text{vap,i}} = \dot{m}_{\text{vap,i-1}} \tag{16}$$

$$R_{\text{en}} = \dot{m}_{\text{liq,i+1}} \cdot h_{\text{liq,i+1}} + \dot{m}_{\text{vap,i-1}} \cdot h_{\text{vap,i-1}} + (\alpha A)_{\text{liq,i}} \cdot (T_{\text{w,i}} - T_{\text{liq,i}}) - \dot{m}_{\text{liq,i}} \cdot h_{\text{liq,i}} - \dot{m}_{\text{vap,i}} \cdot h_{\text{vap,i}} \tag{17}$$

$$d\dot{m}_{\text{vap,i}} = \frac{R_{\text{en}}}{(h_{\text{vap,i}} - h_{\text{liq,i}})} \tag{18}$$

The species balance and other subsequent steps are performed iteratively until convergence on residual energy is achieved. The sequence of steps involved in the desorber solver is summarized in Figure 5. The desorber heat transfer rate is calculated from the net rate of energy change for the solution side in the desorber.

$$\dot{Q}_{\text{DES}} = \dot{m}_{19} \cdot h_{19} + \dot{m}_{16} \cdot h_{16} - \dot{m}_{15} \cdot h_{15} \tag{19}$$

The rectifier is modeled as a simplified heat and mass exchanger with negligible wall and fluid thermal capacities and an assumed outlet concentration of 0.992. The heat is removed from the rectifier by the concentrated solution from the pump. The minimal thermal storage capacity of the rectifier wall and fluid ensures that the heat transfer rate inside the rectifier attains steady-state relatively quickly. Significant rectification is achieved during initial stages of start-up and thus, the assumption of constant outlet concentration is deemed acceptable for this system-level transient model. Component level modeling of the rectifier could incorporate detailed mass transfer modeling to predict the outlet concentration more accurately. Mass, species and energy balances are presented in Equations (20)-(22).

$$\dot{m}_{20} = \dot{m}_{21} + \dot{m}_{22} \tag{20}$$

$$\dot{m}_{20} \cdot X_{20} = \dot{m}_{21} \cdot X_{21} + \dot{m}_{22} \cdot X_{22} \tag{21}$$

$$\dot{m}_{11} \cdot h_{11} - \dot{m}_{10} \cdot h_{10} = \dot{m}_{20} \cdot h_{20} - \dot{m}_{21} \cdot h_{21} - \dot{m}_{22} \cdot h_{22} \tag{22}$$

3.2 Storage Tank Model

Refrigerant and concentrated solution storage in the cycle is modeled using a refrigerant tank and solution tank, respectively. In this model, the tanks represent the numerous heat exchanger headers, sumps, connective tubing, as well as the actual storage tanks present in a physical absorption system. These simulated tanks, allow for expansion and storage of fluid as the system operates at varying conditions throughout the course of start-up, shut-down and different transient conditions. Key assumptions employed in modeling the storage tank are as follows:

- The liquid and vapor phases are in thermodynamic equilibrium at each instant.
- The tank is well-mixed and fluid flowing at the tank outlet is always saturated liquid.
- The pressure inside the tank is communicated to neighboring components in the cycle instantaneously. The low- and high-side pressures are determined by the pressures inside the refrigerant and solution tanks, respectively.

The mass, concentration and specific internal energy of the mixtures inside the tanks are employed to determine the pressures and temperatures of mixtures using liquid-vapor equilibrium relations. The equilibrium pressure
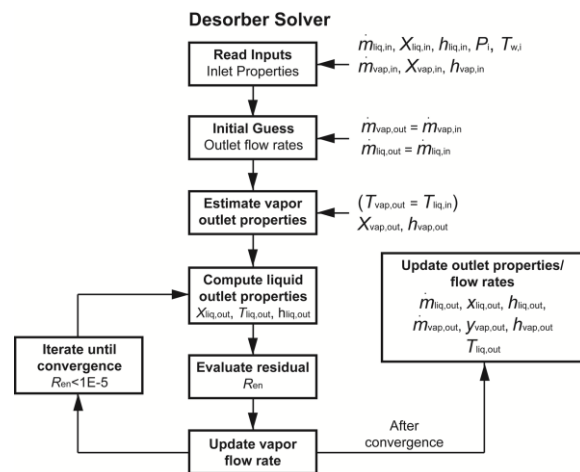
Figure 5: Desorber Solver – Flowchart

inside the refrigerant tank is communicated to the high-side components (DES, COND, RECT and SHX) and the pressure inside the solution tank is communicated to the low-side components (ABS and EVAP).

Mass, species and energy balances are carried out for the mixture inside the refrigerant tank (RT) and the solution tank (ST) (Figure 1):

$$\frac{dm}{dt}\bigg|_{RT} = \dot{m}_{24} - \dot{m}_{25}; \quad \frac{dm}{dt}\bigg|_{ST} = \dot{m}_7 - \dot{m}_8 \tag{23}$$

$$\frac{d(mX)}{dt}\bigg|_{RT} = \dot{m}_{24}\cdot X_{24} - \dot{m}_{25}\cdot X_{25}; \quad \frac{d(mX)}{dt}\bigg|_{ST} = \dot{m}_7\cdot X_7 - \dot{m}_8\cdot X_8 \tag{24}$$

$$\frac{dU}{dt}\bigg|_{RT} = \dot{m}_{24}\cdot h_{24} - \dot{m}_{25}\cdot h_{25}; \quad \frac{dU}{dt}\bigg|_{ST} = \dot{m}_7\cdot h_7 - \dot{m}_8\cdot h_8 \tag{25}$$

3.3 Expansion Valve and Pump
The flow rate of refrigerant through the expansion valve is determined using a flow coefficient model. The model assumes the pressure differential across the valve as the driving force for the flow, and an adjustable flow coefficient, C_{valve}, represents the valve restriction. The expansion valve in the line connecting the absorber and solution heat exchanger is modeled as a simple flow valve which causes a pressure reduction but does not affect other fluid properties.

$$\dot{m}_{ref} = C_{valve}\cdot\sqrt{\Delta P} \tag{26}$$

A constant solution flow rate through the pump is assumed at all times.

3.4 Thermodynamic Properties
The thermodynamic properties of the saturated ammonia-water mixtures are evaluated using property routines developed by Rattner and Garimella (expected submission July 2012). These property routines enable fast and accurate evaluation of state points and are easily accessible from the Matlab® and Simulink® environment. The transient model makes use of these property calls in all of the various components at each time step.

3.5 Solution Methods
Component models are created as re-usable blocks in the Simulink® environment. The ordinary differential equations and other constitutive relations along with the property calls are solved in the Simulink® environment and integrated using the Runge-Kutta algorithm. The time step for numerical integration is limited to a maximum of 0.05 s, and is automatically adjusted to satisfy the relative tolerance of 1×10^{-3} for the residuals of dependent variables.

4. RESULTS AND DISCUSSION

The transient performance of the chiller is discussed in this section. The initial conditions and other parameters for the model are listed in Table 2. An initial temperature of 20°C and a fixed mass of solution and refrigerant determine the initial pressure in the components. The inlet temperatures of the coupling fluids are smoothly ramped from 20°C to their steady state values during the first minute of start-up to minimize the influence of the thermal behavior of the auxiliary systems on the absorption system transient results. The transient performance of the chiller can be characterized in terms of its time-varying heating and cooling loads, pressures, concentrations, and flow rates, as shown in Figure 6. During start-up, the desorber heat load increases sharply, resulting in rapid vapor generation. The other component loads are relatively lower and as a result, the system gradually warms up and attains steady state. The vapor generated in the desorber reaches the condenser wall and raises its temperature. The vapor does not condense completely as the wall temperature is not high enough to reject sufficient heat to the cooling water. Therefore, a two-phase vapor exits the condenser and enters the refrigerant tank during start-up. The vapor accumulates in the refrigerant tank and increases the high-side pressure. This pressure is communicated to

Table 2: Initial Conditions

Quantity	Value
Temperature (°C)	20
Pressure (kPa)	400
Volume of tanks (L)	5
Mass of solution (g)	140
Mass of refrigerant (g)	70
Vapor quality (-)	0.2
Pumping rate (g s⁻¹)	9.75
Valve coefficient (kg s⁻¹ Pa⁻⁰·⁵)	2.54E-6

other components such as the desorber, condenser and rectifier. Figure 6 shows a sharp increase in the desorber heat load and a resultant increase in the high-side pressure.

Saturated liquid ammonia-water mixture drains out of the refrigerant tank and flows through the expansion device to the evaporator. The pressure differential across the valve governs the refrigerant flow rate. The pressure differential is initially zero; therefore, the refrigerant flow rate starts at zero and increases as the high-side pressure rises. The evaporator temperature is close to the ambient temperature during start-up. It decreases as the high-side pressure increases, and more liquid-phase refrigerant is expanded from the refrigerant tank to the evaporator pressure. As a result, the evaporator cooling duty is low initially, and the evaporator exit quality is low for the first minute of operation. The two-phase mixture flowing from the evaporator outlet is further heated in the RHX before it reaches the absorber. The initially low refrigerant flow rate causes the absorber cooling load to lag behind the desorber heating rate. The hot dilute solution exiting the desorber only experiences a small amount of cooling in the SHX initially. Thus, sensible cooling of solution accounts for a large fraction of the absorber heat load during the initial stages of start-up. The absorber rejects this heat to the cooling water and the cooled ammonia-water solution enters the solution tank. The quality of the mixture exiting the absorber is initially low due to the reduced vapor flow rate at the absorber inlet. The mixture flows out of the absorber at low quality and enters the solution tank. The pressure in the solution tank (low-side pressure) increases comparatively slowly with increasing refrigerant vapor flow rate at the evaporator outlet.

Table 3: Steady-State Data

Quantity	Value
Heat load of components (kW)	
DES	5.7
ABS	5.54
EVAP	3.45
COND	3.61
Flow rates of solution (g s^{-1})	
Concentrated sol	9.75
Dilute sol	6.7
Refrigerant	3.1
Cycle pressure (kPa)	
High-side	1946
Low-side	463
Concentration of solution	
Ammonia-vapor	0.9917
Concentrated sol	0.479
Dilute sol	0.2423

The concentrations of dilute solution exiting the desorber and concentrated solution entering the desorber are shown in Figure 6. The concentration of solution entering the desorber is equal to that of the solution draining from the solution tank, and is approximately 0.62 at t = 0. As the desorber warms up, generation of ammonia-vapor reduces the dilute solution outlet concentration. The refrigerant concentration shown in Figure 6 is that of ammonia-water mixture flowing out of the refrigerant tank. Initially, the concentration of ammonia inside the refrigerant tank is 0.69, but as time progresses, the ammonia-vapor generated in the desorber accumulates in the refrigerant tank and increases its concentration to the steady state value of 0.992. During the initial stages of start-up, the net heat load increases and attains a maximum as the system warms up. The condenser heat load increases sharply after approximately t = 40 s owing to a drastic reduction in quality of the ammonia-water mixture exiting the condenser. It results in significant reduction of net heat load at around t = 40 s. After t = 120 s, the system approaches steady-state, which is further confirmed by a zero net heat load. During steady state, the evaporator cooling rate is 3.45 kW, and the condenser load is nearly equal to 3.6 kW. The absorber and desorber heat transfer rates are also nearly equal (5.6 kW). The steady-state results are summarized in Table 3. Overall, these values match closely with results from a steady state system model with equivalent input data such as component sizes, heat transfer coefficients, system flow rates, and operating conditions.

5. CONCLUSIONS

A transient model of a small-capacity absorption chiller was developed in this study. The thermal storage capacity of heat and mass transfer components, refrigerant and solution storage, flow rate development through the valves, etc. are accounted for in the transient behavior. The component sizes, thermal storage capacities, coupling-fluid flow rates and temperatures used here are representative of a miniaturized absorption system being developed by the authors. Segmented models of heat and mass transfer components, instead of lumped capacitance models typically used in the literature, were employed to model transient phenomena with high fidelity. The storage tanks were modeled to account for expansion and storage of fluid during start-up, shut-down and other transient events. The equilibrium pressures inside the refrigerant and solution tanks were communicated as high-side and low-side pressures, respectively. Results from the transient analysis indicate that parameters such as flow rates, pressures and concentrations attained their steady state values in approximately three minutes. The desorber heat load increased rapidly, followed by the absorber load and the condenser and evaporator loads. The evaporator and condenser
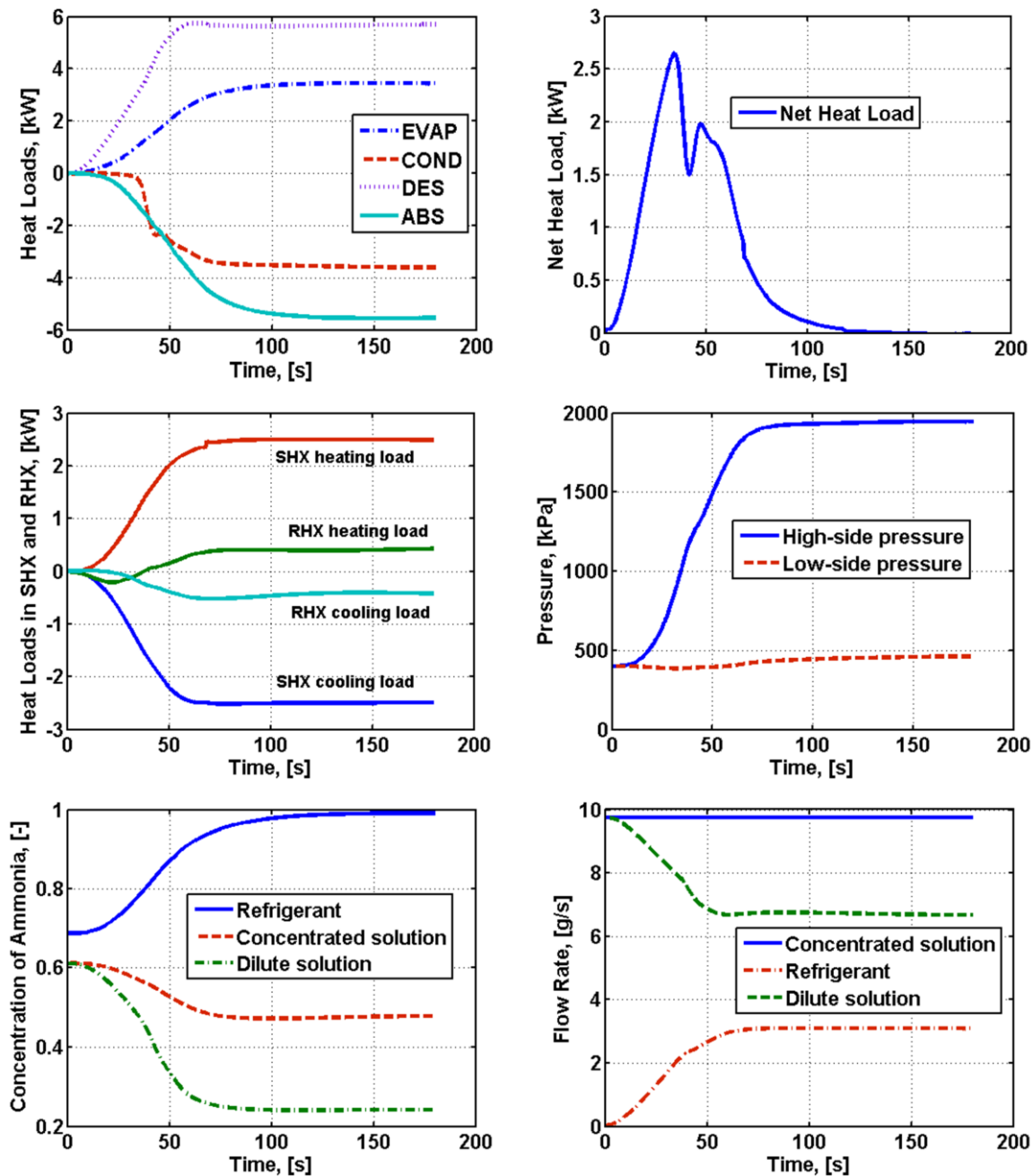
Figure 6: Transient performance characteristics

required additional time to reach steady state. The evaporator heat load is 3.45 kW at steady state for the given set of component sizes and pumping rate. The effect of system parameters such as heat exchanger size, solution flow rates, specific pump curves, coupling fluid temperatures and flow rates on the transient performance of the absorption system can be studied in detail using the model developed in this work. Future work will incorporate additional sub-models accounting for varying thermal capacity of coupling fluid lines and ambient heat exchangers and could be employed to predict transient performance under various scenarios for a specific installation of the chiller.

NOMENCLATURE

A	area	(m^2)		**Subscripts**	
C_{valve}	valve coefficient	$(kg\ s^{-1}\ Pa^{-1})$	cf	coupling fluid	
c_p	heat capacity	$(J\ kg\ K^{-1})$	f	fluid	
h	enthalpy	$(J\ kg^{-1})$	HX	heat-exchanger	
M,m	mass	(kg)	liq	liquid	
$\dot{m}$	mass flow rate	$(kg\ s^{-1})$	seg	segment	
N	number of segments	$(-)$	sol	solution	
$P, \Delta P$	pressure, pressure differential	(kPa)	vap	vapor	
$\dot{Q}$	heat transfer rate	(W)	w	wall	
T	temperature	(^{o}C)			
t	time	(s)			
U	extensive internal energy	(J)			
X	concentration of ammonia	$(-)$			
α	heat transfer coefficient	$(W\ m^{-2}\ K^{-1})$			

REFERENCES

Cai, W., M. Sen and S. Paolucci, 2011, Dynamic Simulation of an Ammonia–Water Absorption Refrigeration System, *Industrial & Engineering Chemistry Research*, vol. 51, no. 4: p. 2070-2076.

Determan, M. D. and S. Garimella, 2012, Design, Fabrication, and Experimental Demonstration of a Microscale Monolithic Modular Absorption Heat Pump, *Applied Thermal Engineering*, vol. 47, no. 0: p. 119-125.

Fu, D. G., G. Poncia and Z. Lu, 2006, Implementation of an Object-Oriented Dynamic Modeling Library for Absorption Refrigeration Systems, *Applied Thermal Engineering*, vol. 26, no. 2–3: p. 217-225.

Jeong, S., B. H. Kang and S. W. Karng, 1998, Dynamic Simulation of an Absorption Heat Pump for Recovering Low Grade Waste Heat, *Applied Thermal Engineering*, vol. 18, no. 1–2: p. 1-12.

Kaushik, S., N. Sheridan, K. Lam and S. Kaul, 1985, Dynamic Simulation of an Ammonia-Water Absorption Cycle Solar Heat Pump with Integral Refrigerant Storage, *Journal of Heat Recovery Systems*, vol. 5, no. 2: p. 101-116.

Kim, B. and J. Park, 2007, Dynamic Simulation of a Single-Effect Ammonia–Water Absorption Chiller, *International Journal of Refrigeration*, vol. 30, no. 3: p. 535-545.

Kohlenbach, P. and F. Ziegler, 2008, A Dynamic Simulation Model for Transient Absorption Chiller Performance. Part I: The Model, *International Journal of Refrigeration*, vol. 31, no. 2: p. 217-225.

Patankar, S. V., 1980, *Numerical Heat Transfer and Fluid Flow*, Hemisphere Publishing Corporation, Taylor and Francis Group, New York, p.

Rattner, A. S. and S. Garimella, expected submission July 2012, Fast, Stable Computation of Thermodynamic Properties of Ammonia-Water Mixtures, *International Journal of Refrigeration*.

ACKNOWLEDGEMENT